nature communications

Article

https://doi.org/10.1038/s41467-025-57982-5

Biogel scavenging slows the sinking of organic particles to the ocean depths

Received: 25 August 2024

Accepted: 7 March 2025

Published online: 07 April 2025

Check for updates

Uria Alcolombri[1] ✉, Alon Nissan[2], Jonasz Słomka[3], Sam Charlton[3], Eleonora Secchi[3], Isobel Short[3], Kang Soo Lee[4], François J. Peaudecerf[5], Dieter A. Baumgartner[3], Andreas Sichert[6], Uwe Sauer[6], Anupam Sengupta[7,8] & Roman Stocker[3] ✉

One of Earth's largest carbon fluxes is driven by particles made from photosynthetically fixed matter, which aggregate and sink into the deep ocean. While biodegradation is known to reduce this vertical flux, the biophysical processes that control particle sinking speed are not well understood. Here, we use a vertical millifluidic column to video-track single particles and find that biogels scavenged by particles during sinking significantly reduce the particles' sinking speed, slowing them by up to 45% within one day. Combining observations with a mathematical model, we determine that the mechanism for this slowdown is a combination of increased drag due to the formation of biogel tendrils and increased buoyancy due to the biogel's low density. Because biogels are pervasive in the ocean, we propose that by slowing the sinking of organic particles they attenuate the vertical carbon flux in the ocean.

The sinking of photosynthetically fixed carbon in the form of organic particles to the oceans' depths drives one of the largest carbon fluxes in the carbon cycle, the biological gravitational pump (BGP)[1]. Along with other processes that are collectively termed the biological pump, this mechanism generates a significant downward flux of carbon from the ocean surface to its interior, estimated at 50–60 Gt yr^{-1} (refs. 1–3). However, the fate of these sinking particles is intricately tied to processes of consumption and degradation by zooplankton and bacteria, leading to the conversion of organic carbon into biomass or its remineralization back into carbon dioxide[4–7]. Consequently, only a fraction of the fixed carbon leaves the euphotic zone, and ~1% reaches the sediments for long-term sequestration[8–10]. The amount of carbon sequestered in the oceans via the gravitational pump is, therefore, principally determined by the balance between two opposing processes – particle sinking and particle degradation – which are in turn influenced by biotic and abiotic factors that change as the particles descend through the water column[5,11–13]. Yet, due to the major challenge of following particles' sinking speed while observing their transformation through the water column, the factors that determine particles' sinking speed and the mechanisms involved in their acceleration or deceleration during descent remain underexplored.

Particles encounter and scavenge large quantities of biomass as they sink through the ocean water column[14,15]. This biomass often includes suspended material and biogels[16–19], gel-like matrices of biological origin, which may change the size, shape, and composition of the particles. For instance, among marine biogels, the micro-gels fraction (3–6 μm size range) alone represents one of the largest standing stocks of carbon in the oceans, equivalent in mass to the living part of the entire global marine biomass, with concentrations ranging from 10^6 to 3×10^{12} micro-gels L^{-1} and distribution spanning depths from 10 to 4000 m[20]. Biogels can range in size from nanometers to centimeters and have diverse sources, including direct

[1]Institute for Life Sciences, Department of Plant and Environmental Sciences, The Hebrew University of Jerusalem, Jerusalem, Israel. [2]The Robert H. Smith, Faculty of Agriculture, Food and Environment. Department of Soil and Water Sciences. The Hebrew University of Jerusalem, Rehovot, Israel. [3]Institute of Environmental Engineering, Department of Civil, Environmental and Geomatic Engineering, ETH Zurich, Zurich, Switzerland. [4]Department of Mechanical Engineering, Ulsan National Institute of Science and Technology (UNIST), Ulsan, South Korea. [5]Univ Rennes, CNRS, IPR (Institut de Physique de Rennes) - UMR 6251, Rennes, France. [6]Institute of Molecular Systems Biology, Department of Biology, ETH Zurich, Zurich, Switzerland. [7]Physics of Living Matter Group, Department of Physics and Materials Science, University of Luxembourg, Luxembourg City, Luxembourg. [8]Institute for Advanced Studies, University of Luxembourg, Esch-sur-Alzette, Luxembourg. ✉e-mail: Uria.Alcolombri@mail.huji.ac.il; romanstocker@ethz.ch

autotrophic production, biofilms, and self-assembled from dissolved organic matter[20–27]. Moreover, biogels are expected to increase in abundance due to anthropogenic activities, higher CO_2 levels, and acidification, which is predicted to result in shifts in community composition, increased rates of primary productivity, and enhanced extracellular release of organic compounds[17,22,24,28]. The biogel standing stock contributes to particle coagulation in the mixing layer and facilitates their transfer to the mesopelagic[25,29]; however, the effects of biogels on the gravitational sinking of particles in the mesopelagic remain unclear, and a better knowledge of the interplay between biogel standing stock and sinking particles is important to improve our understanding of processes that regulate the biological pump.

Here, we quantify the impact that biogel accumulation on marine organic particles due to the sinking of the particles has on the particles' sinking speed. We use suspended bacterial biofilm aggregates as a naturally relevant model of suspended biogels and laboratory-made algal aggregates as a model of organic particles. Using a millifluidic device that allows for long-term imaging and tracking of single sinking particles in the laboratory, we demonstrate that suspended biofilms adhere to and accumulate on particles in large amounts as these sink through seawater. We find that, despite increasing the particles' volume (which by itself would increase the sinking speed), this accumulation induces a substantial slow-down of the particles, reducing their sinking speed by up to 45% within one day. Using a mathematical model to interpret our observations, we find that the mechanism for the slow-down is a combination of an increase in drag due to the elongated tendrils formed by biogel accumulation, which increase hydrodynamic resistance to sinking, and an increase in buoyancy due to the biogels having a lower density than the particles. Owing to the broad distribution of biogels in productive regions of the ocean, we propose that biogel accumulation on particles can attenuate the vertical carbon flux in the ocean, providing additional mechanistic insight into the role of biogels in the oceanic carbon cycle.

Results and discussion

Biogel accumulation on marine particles slows their sinking

To quantify the effect of the encounter and attachment of suspended biogels on the sinking speed of particles, we developed an 'endless-ocean column' device that allows for the long-term visualization and tracking of individual particles as they sink (Fig. 1A and Supplementary Fig. 1–3). This device, which was developed based on inspiration from Ploug et al. [30], is composed of a 20 cm-long vertical glass tube of square cross-section (0.5 cm × 0.5 cm), connected to a seawater reservoir and containing an organic particle that is suspended at the center of the tube. The particle is kept in suspension by a pump that generates an upward flow in the tube of a magnitude that exactly matches the instantaneous sinking speed of the particle so that the particle remains stationary in the field of view of a camera. The flow rate delivered by the pump is controlled via a computer program that uses real-time analysis of images from a second camera to determine the shift in the vertical position of the particle and uses this to adjust the pump's flow rate. Using this approach, we were able to image single particles continuously for up to two days and obtain their time-resolved sinking speed from the temporal evolution of the flow rate of the pump (Methods).

When we investigated model particles sinking in artificial seawater (ASW with 0.1% 2216 Marine Broth, "Methods") containing *Alteromonas macleodii* ATCC 27126, a common biofilm-forming marine bacterium and a model system to study biofilm aggregates (see Supplementary Text, Supplementary Figs. 4, 5 and Supplementary Movie 5)[31,32], we found that the particle sinking speed decreased substantially over the course of 24 h. In contrast, only minor or no changes in particle sinking speed were observed when ASW was amended with a non-biofilm-producing bacterium, *Vibrio cyclitrophicus* 1F111[33], or in the absence of bacteria (Fig. 1B, C and Supplementary Fig. 2, $n = 4$, 2 and 5 respectively). The particles used in these experiments were obtained by rolling culture tubes of the alga *Phaeodactylum tricornutum* on a tube roller for 3–7 days at 20 rotations/min, resulting in particles with a diameter of 0.1–0.6 mm. Prior to experiments, *A. macleodii* bacteria were grown for 48 h in marine broth at 27 °C. This resulted in a culture that contained approximately one suspended biofilm aggregate for every 10 free-living cells, as estimated by microscopy. The culture was diluted in ASW to a final concentration of $(3.1 \pm 1.8) \times 10^9$ CFU/L, and this suspension was flown through the endless-ocean column for the duration of the experiment. The concentration of bacteria in the reservoir after 24 h was found to be $(4.2 \pm 2.2) \times 10^9$ Colony forming units per liter (CFU/L), indicating little growth in the reservoir during the course of the experiment. The estimated concentration of biofilm aggregates used in the experiments was thus $(3.1 \pm 1.8) \times 10^8$ biofilm-aggregates/L, a concentration similar to that of biogels in coastal and productive zones of the ocean[34]. Microscopy showed that *A. macleodii* biofilm aggregates had a mean diameter of 15 μm (5–220 μm) and resembled in size and shape suspended biogels observed in seawater[22,35,36]. A chemical analysis of the composition of *A. macleodii* biofilm aggregates and a bioinformatic survey of *A. macleodii*'s genome to identify the genes involved in its production revealed further similarities to naturally occurring marine biogels (Supplementary Text and Supplementary Data 1).

In the presence of *A. macleodii*, particles sank at first at a speed of 43–98 m/day ($n = 4$), then gradually slowed to 34–52 m/day over 20–24 h, representing a 25–46% reduction in sinking speed. The sinking speed decreased linearly over the 24 h of observation, indicating that the process responsible for the slowdown unfolded progressively over time and had not reached saturation by the end of the observation period. Generally, experiments with *A. macleodii* ended when the particle tracking algorithm failed, usually around 24 h after the experiment started (Fig. 1B). Images of the particles acquired every 5 min for the entire duration of each experiment revealed that the reduction in sinking speed was accompanied by an accumulation of biofilm aggregates on the particles, which modified their shape and increased their size (Fig. 1D, E, Supplementary Fig. 3 and Supplementary Movie S1). Based on these single-particle observations, we hypothesized that the scavenging of bacterial biofilm aggregates by a particle is the mechanism responsible for the particle's reduction in sinking speed.

To further test this hypothesis, we performed two additional sets of experiments. In the first, we used a bulk experiment to assay a substantially larger number of particles. For these experiments, particles pre-made from *P. tricornutum* cultures (using the same methodology as in the endless-ocean column experiments) were incubated for 48 h in a rolling tube in the presence or absence of a stationary *A. macleodii* culture, diluted to the same concentration as in the endless-ocean-column experiments (Methods). Particles were then gently loaded in batches at the top of a sedimentation chamber (15 cm high × 1 cm wide × 0.6 cm deep) filled with ASW, and their terminal sinking speed was measured by imaging (Supplementary Fig. 6 and Supplementary Movie 2, "Methods"). This provided a coarser-grained but higher-throughput measure of the impact of biofilm aggregates on particle sinking speed. In agreement with the single-particle experiments in the endless-ocean column, particles incubated with *A. macleodii* had an average sinking speed 17% lower than particles incubated without *A. macleodii*, despite having an 8% larger effective radius (ER) (Fig. 1F, G; $p < 0.0002$, Mann-Whitney test, $n = 1464$ and 642 particles, respectively), where the ER is the radius of a spherical particle that has the same cross-sectional area as the particle (where the cross-sectional area is quantified from imaging data). This result confirms that biogel scavenging reduces particle sinking speed.

In the second set of experiments, we determined through microscopy the prevalence of biofilm-forming bacteria among a collection of 96 strains isolated from marine particles[37]. We found that 14 out of the 96 strains produced biofilms under laboratory conditions

https://doi.org/10.1038/s41467-025-57982-5

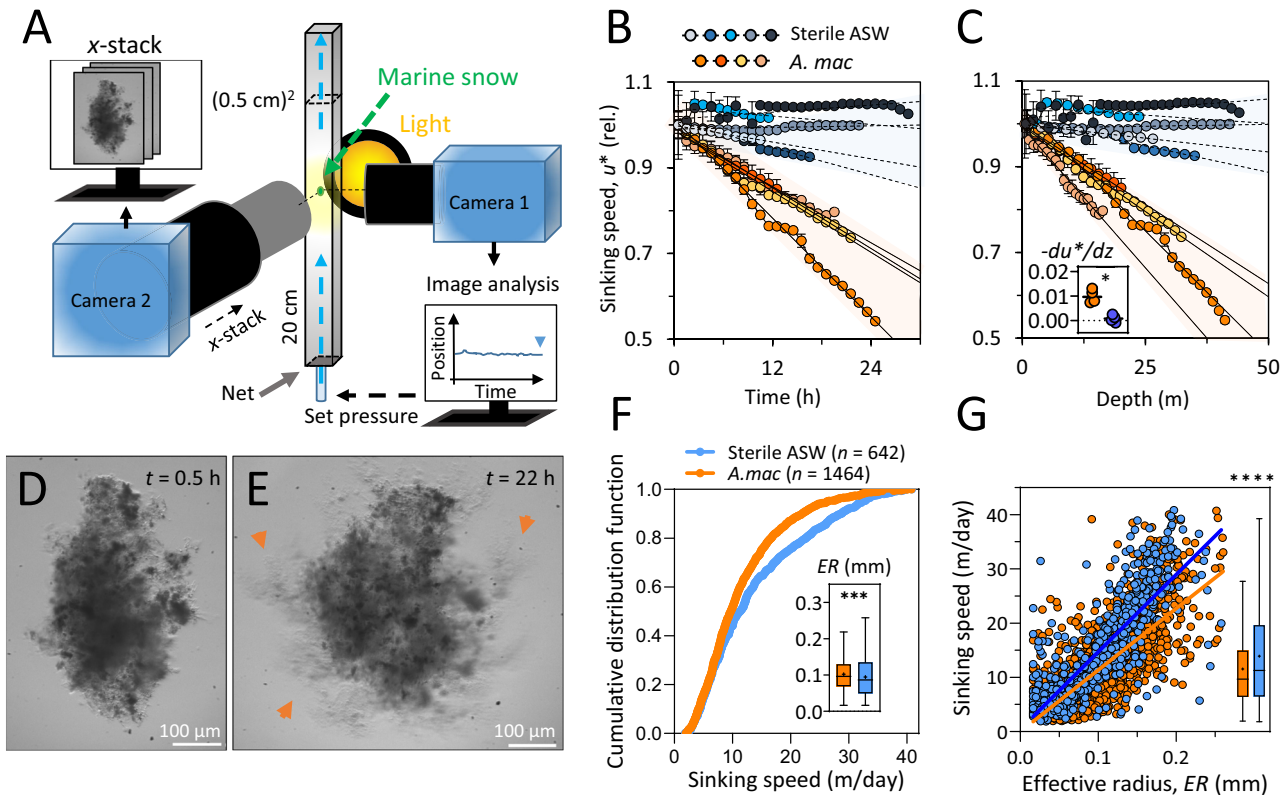

Fig. 1 | *Alteromonas macleodii* biofilm aggregates slow down the sinking of marine snow particles. A Schematic of the 'endless-ocean column' device used to track the sinking speed of an individual particle over extended periods of time. The upward flow rate through the column is continuously adjusted (through feedback from its instantaneous position recorded by camera 1) to maintain an otherwise freely sinking particle suspended at a fixed location (8–10 cm above a 100 µm-mesh net that is placed at the base of the device to act as a flow homogenizer) for video microscopy imaging (using camera 2, which acquires a stack of images at different x positions to capture the best in-focus image). **B**, **C** The particle sinking speed measured in the endless-ocean column decreases linearly with time (**B**) and thus also with equivalent sinking depth (**C**) in the presence of *A. macleodii* (yellow and orange shades, $n = 4$), whereas it changes only by minute amounts over time in sterile artificial seawater (gray and blue shades, $n = 5$). The sinking speed u^* relative to the initial sinking speed is plotted. The sinking speed values are presented as hourly averages. The bars represent the standard deviation calculated over the 1 h interval. Thin black lines are linear fits for each curve. (**C** inset) Vertical deceleration $-du^*/dz$, obtained from the slope of each curve. The asterisk denotes a statistically significant difference (Welch's t test, $n = 4$ and 5, p-value < 0.01). **D**, **E** A marine snow particle at two time points (0.5 h and 22 h) during a sinking experiment. Orange arrows denote *A. macleodii* biofilm aggregates that have accumulated on the particle. Images for the no-bacteria control experiment are shown in Supplementary Fig. 3. **F**, **G** Sinking speed of particles measured in a sedimentation chamber (Supplementary Fig. 6) after incubation with *A. macleodii* (orange, $n = 1464$) or sterile artificial seawater (ASW, blue, $n = 642$). (**F**) Cumulative distribution functions of sinking speed of particles. (Inset) Box-and-whisker plot of the effective radius of the particles (ER; see text for definition). The difference is statistically significant (p-value < 0.0002, two-tailed Mann–Whitney test). (**G**) Sinking speed of the same particles of panel F shown as a function of the particles' ER. Color-coding as in panel **F**. The difference in sinking speed is presented with box-and-whisker plots on the right and is statistically significant (p-value < 0.0001, two-tailed Mann–Whitney test). Box-and-whisker plots are based on Tukey's method, the median is indicated with a line and the mean with a plus. Source data are provided as a Source Data file.

(Supplementary Fig. 8 and Supplementary Text). We then tested two such biofilm-forming strains in the endless-ocean column for 40–60 h. We observed that one strain, *Pseudomonas zhaodongensis* S15, also slowed particle sinking by producing biofilm aggregates, whereas the other strain, *Bacillus* sp. F2, did not (Supplementary Fig. 7). Further analysis in a high-magnification microfluidic setup revealed that *Bacillus* sp. F2 produced thin, mechanically weak biofilms, which did not accumulate on particles because they were sheared off by fluid flow (Supplementary Movie 3). Together, these experiments indicate that the accumulation of biofilm aggregates on particles is responsible for the particles' slowdown. Yet, not all biogels have the mechanical resilience to accumulate on and slowdown particles, highlighting the importance of better understanding the role of the biofilm's material properties in this process.

Biogel-induced particle slowdown originates from a combination of density reduction and drag increase

The accumulation of *A. macleodii* biofilm aggregates on particles reduced the particles' overall density (i.e., it increased their overall buoyancy). To determine the difference in density between the particles and the biofilm aggregates, we used a Percoll density gradient to separately measure the density of bacteria-free particles made from *P. tricornutum* and the density of *A. macleodii* biofilm aggregates (collected from MB 2216 medium during stationary growth, Methods). The excess density $\Delta\rho$ (relative to ASW) of the biofilm aggregates was 0.005 kg/L, indicating that the biofilm aggregates were almost neutrally buoyant. This excess density was more than 20-fold smaller than the excess density of the particles, $\Delta\rho > 0.105$ kg/L (which represents the maximum density measurable using the Percoll gradient method, Supplementary Fig. 9). This density difference implies that the accumulation of biofilm aggregates on particles decreases the particles' overall density, which by itself (*i.e.*, separately from the increase in particle volume) based on Stokes' law[38] acts to cause a decrease in sinking speed. In addition, we measured the density of *A. macleodii*, both for planktonic, exponentially growing cells and for stationary-state biofilm aggregates. We found that planktonic cell density decreases as cells approach the stationary phase and form biofilm aggregates (Fig. 2A–C and Supplementary Fig. 9; $\Delta\rho = 0.034$ kg/L for

https://doi.org/10.1038/s41467-025-57982-5

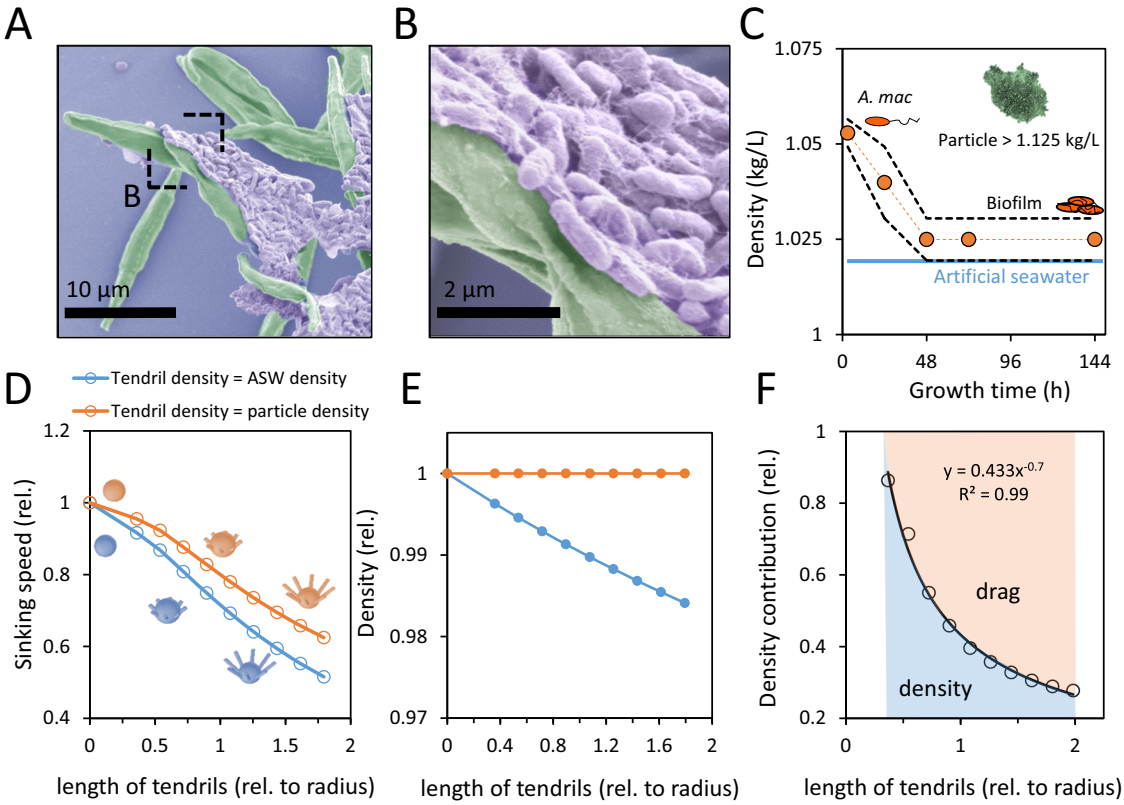

Fig. 2 | Increased buoyancy and drag cause the biogel-accumulation induced slowdown. A, **B** False-color scanning electron microscope (SEM) image of a layer of *A. macleodii* biofilm aggregates (purple) on a laboratory-made marine snow particle. *Phaeodactylum tricornutum* cells used to make the particle are shown in green. **C** The density of *A. macleodii* biofilm aggregates measured in a Percoll density gradient at different growth stages (planktonic exponential $t = 0–48$ h to biofilm stationary $t = 48–144$ h). The orange line shows *A. macleodii* mean density values. The densities of the layers below, and the one containing the biofilm band are indicated by black dashed lines. The density of artificial seawater is shown by the blue line. Inset: density of the diatom-made particles used in experiments. **D**, **E** The sinking speed (**D**) and density (**E**) of particles as a function of the length of biofilm-aggregate tendrils projecting from the particle surface (as shown by the inset images), obtained from a mathematical model (Supplementary Materials). Both sinking speed and density are shown relative to the case of no tendrils, and the length of tendrils is normalized to the radius of the (tendril-free) particle. Particle sinking was modeled under two scenarios: in blue, the tendrils' density is equal to that of seawater, and in orange, the tendrils' density is equal to that of the particles themselves. **F** The estimated contribution of declining density to the overall deceleration of particle sinking. Source data are provided as a Source Data file.

planktonic bacteria and $\Delta\rho = 0.005$ kg/L for biofilm aggregates). This indicates that the exopolymeric substances (EPS) produced by the bacteria during biofilm formation, together with the incorporated cells, contribute to the low excess density of the biofilm aggregates. This small excess density of *A. macleodii* biofilm aggregates is in line with the excess density of transparent exopolymer particles (TEP) and other biogels commonly found through the water column, which have been reported to have neutral or even negative excess densities[17,39]. Together, these findings demonstrate that attachment of biofilm aggregates, and by extension other biogels, to marine particles can decrease the density of particles, thus acting to reduce their sinking speed. As we show below through a mathematical model, the increase in particle volume that also results from biogel scavenging is not sufficient to counteract this slowdown.

In addition to a decrease in density, a second mechanism contributed to the observed slowdown of particles. Our observations showed that biofilm aggregates did not accumulate on a particle uniformly, but rather by forming local protrusions (henceforth, 'tendrils') that often elongated. Scanning electron microscopy (SEM) images of biofilm aggregates attached to a particle revealed that the aggregates are made of thin layers of *A. macleodii* cells entangled within a matrix of EPS (Fig. 2A, B). The tendrils considerably increased the surface area of the particle (Supplementary Movies 1, 3–5), which acts to increase the hydrodynamic resistance to sinking (*i.e.*, the drag). On the other hand, the increase in the volume of the particle, observed in the endless-ocean column (Fig. 1E) and quantified in the bulk sedimentation experiments (Fig. 1F), would act to increase its sinking speed, based on Stokes' law[38].

To corroborate the hypothesis that tendrils slow the sinking despite the increase in particle volume, we developed a mathematical model to quantify the impact of the density and size of biogels on the sinking speed of a particle (Fig. 2D, E, Supplementary Fig. 10 and Supplementary Materials). The model mimics the presence of tendrils observed in experiments by considering a spherical particle decorated with equal-length tendrils on its surface. For simplicity, we assumed the particle and the tendrils to be rigid. We simulated eight tendrils protruding at a 45-degree angle (relative to the vertical axis) to represent the observed tendency of biogel accumulations to extend into the flow and particularly into the wake, yet we also performed additional simulations showing that the main conclusions are robust to variations in the number, thickness and angle of tendrils (Supplementary Materials and Supplementary Fig. 10). By comparing the sinking speeds of particles with tendrils of different densities—either matching the density of water (as observed in biogels) or matching the particle's density (thus not affecting the particle's overall density)— we found that biogel tendrils cause a large reduction in sinking speed and that this occurs even in the latter case, *i.e.*, when no change in the particle's density occurs (Fig. 2D, E, in orange). Overall, this means that

https://doi.org/10.1038/s41467-025-57982-5

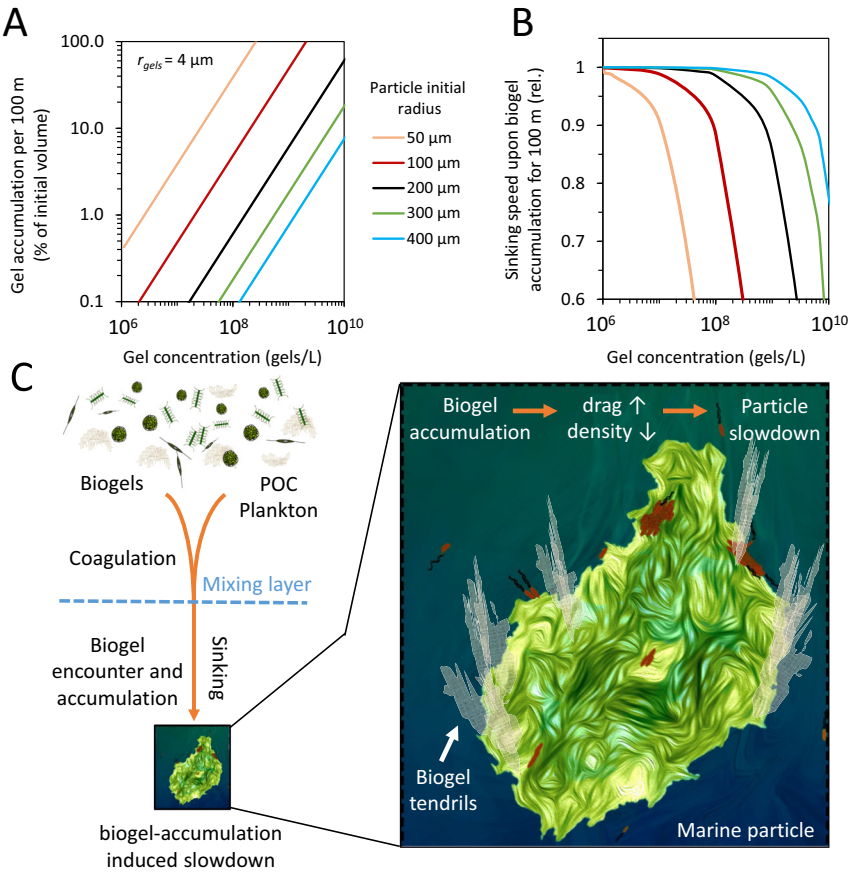

Fig. 3 | Predicted effect of biogel-accumulation-induced slowdown in the natural environment. A Model-based prediction of biogel accumulation on a marine particle (as percentage of the initial particle volume) as the particle traverses 100 m of depth as a function of the biogel concentration in seawater (for a biogel radius of 4 µm) for particles of different initial radii (color-scale). Note that results are independent of the particle sinking speed because they are presented per 100 m of depth and because biogel interception occurs at low Reynolds numbers. See Supplementary Materials for details. **B** Model-based prediction of the reduction in sinking speed resulting from the biogel volume addition in (**A**). **C** Schematic of the proposed mechanism of biogel-accumulation-induced slowdown of marine particles. In the surface ocean, biomass aggregation into sinking particles is facilitated by sticky biogels, including biofilm aggregates, TEP, and EPS. Once below the mixing layer, particles are exposed to very weak turbulence and collect biogel tendrils on their surface as they sink. Biogel tendrils increase hydrodynamic resistance and decrease the overall density of particles. This, in turn, slows their sinking, exposing them to degradation and remineralization for longer and potentially decreasing the carbon sequestered in the ocean depths. Source data are provided as a Source Data file.

as tendrils elongate, not only the changes in density due to the low excess density of most biogels, but also the increased drag due to the often-elongated nature of tendrils contribute to slow down the particle. The model further revealed that, as tendrils become longer, causing both the overall particle density and drag to change (Fig. 2D, E, in blue), the relative contribution of buoyancy to the overall slowdown declined, saturating at around 30% (Fig. 2F). Notably, the model also predicts that the magnitude of the slowdown is linearly proportional to the length of the tendrils, which is in line with the observed linear decrease in sinking speed and the expectation that biogel accumulation occurs approximately linearly in time (Fig. 1B, C). Overall, our model predicts that the addition of biogel tendrils to a particle not only makes the particle more buoyant but also increases its drag, outweighing the opposing effect of increased particle volume, which would otherwise accelerate the particle due to greater gravitational force.

Environmental implications of biogel accumulation on marine particles

The decelerating effect on marine particles of biogels and biofilm aggregates is likely to vary depending on the concentrations and sizes of these entities in the water column, which in turn will vary with ocean region and environmental parameters such as water temperature, season, and eutrophication[17,34]. To estimate the effect of biogel accumulation on sinking particles under different environmental conditions, we calculated the amount of biogels expected to accumulate on a particle that sinks at speed $U_{sinking}$ through seawater containing different concentrations of biogels, C_{gel} (Fig. 3A). Modeling the particle as a sphere and assuming that biogel aggregates are small (equivalent radius r_{gel}; Reynolds number $Re < 1$[38]) and thus encountered by a particle through direct interception, the particle–gel encounter rate is predicted to be $E = 1.5\pi C_{gel} U_{sinking} r_{gel}^2$ [40]. Using the particles sinking speed–volume relationship obtained from our mathematical model (Fig. 2D and Supplementary Materials), we estimated biogel accumulation on particles per 100 m depth (assuming all biogels stick upon encounter) and its impact on sinking speed under varying biogel concentrations and sizes. Accordingly, a 200 µm-radius particle sinking at 30 m/day ($Re = 0.05$) in seawater containing 2×10^9 biogel-aggregates/L with an estimated biogel radius $r_{gel} = 3–4$ µm, typical for example of Bermuda Atlantic water during the summer[34], is predicted to collect an amount of biogels equal to 3–12% of its original volume for every 100 m of depth it traverses (black line in Fig. 3A, B and Supplementary Fig. 11). This volume addition is substantial and is predicted to result in a sinking speed reduction of 7–29% for every 100 m of depth

(Supplementary Materials). Seawater containing smaller concentrations of biogel aggregates (3×10^8 biogel-aggregates/L), like at station ALOHA in the North Pacific[34], would result in a sinking speed reduction of 1–4% per 100 m of depth for the same values of gel size r_{gel} (Supplementary Fig. 11), which is more modest but can still have a significant impact on the vertical carbon flux, particularly when integrated over many hundreds of meters of depth. As a further example, in a coastal bloom scenario with 3×10^8 biogel-aggregates/L[41] of larger size ($r_{gel} = 7$ μm), the predicted slowdown is very large at 71% per 100 m. To our knowledge, data on the efficiency of the adhesion of biogels to particles is currently unavailable. Moreover, marine snow aggregates are composed of plankton that produce EPS with varying quantities and adhesive characteristics, influenced by their taxonomic origin and physiological state[42–44]. Different degrees of adhesion could impact the efficiency of biogel accumulation on particles and, consequently, influence their ability to reduce particle sinking speeds. Our model assumes 100% attachment upon encounter, representing the upper limit of the effect of biogels on particle sinking. In addition, in the environment, biogels may also adhere to other locations, including the upstream half of the particle, adding complexity not captured in our model (Supplementary Materials). A more comprehensive understanding of the adhesive properties of various biogels and particle types will be important to gain a more nuanced quantitative understanding of this phenomenon. Nevertheless, these calculations suggest that the biogel standing stock is an important determinant of particle sinking speed and that this can have potentially major consequences on the flux of carbon to depth.

The variability of microgel concentration with depth and geographic location is an important factor that can significantly influence particle settling velocity. Yet, field measurements of microgel concentrations, particularly their variation with depth, remain scarce. For this study, we used a concentration of about 10^9 biogel-aggregates/L based on available data for oligotrophic regions such as Bermuda Atlantic Time-series Study (BATS)[34], but concentrations as low as 10^7 biogel-aggregates/L have been observed in deeper waters or different environmental conditions[34]. This range highlights the diverse conditions under which microgels exist in the water column and, thus, the variability of their impacts on sinking particles. For example, reduced microgel concentrations at greater depths could lessen their effect on particle settling velocity. Conversely, surface conditions during large phytoplankton blooms, where both microgel and bacterial concentrations are typically elevated, may enhance biogels' impact on slowing particle descent in the upper water column. By presenting our findings as a function of biogel concentration (Fig. 3), we provide a basis for understanding how microgel variability may shape particle dynamics across different oceanographic conditions while emphasizing that a broader range of empirical data on microgel concentration across depth, geographic location and bloom events are needed to fully be able to predict the magnitude of this effect.

Our findings on the biogel-induced particle slowdown find support in recent field observations[45–47]. In a recent study in the Gulf of Maine, marine particles were collected using sediment traps at 80 m depth and analyzed in situ using scale-free vertical tracking microscopy and particle image velocimetry (PIV)[48]. This analysis revealed that transparent exopolymer particle (TEP) tails on the particles, akin to the tendrils we observed, significantly distort the flow around the particles, causing an expected (but not directly measured relative to tendril-free particles) reduction in sinking speed by half[47]. A summertime campaign in the oligotrophic Northeast Pacific reported particles that were not sinking despite substantial ballast content. Approximately 15% of the carbon in these particles was attributed to TEP, a feature that was associated by the authors with their slow to non-existent sinking behavior[45]. Sampling campaigns in regions experiencing spring phytoplankton blooms, including near Hokkaido and the oligotrophic subtropical Kuroshio region, revealed similar results based on the use of marine snow catchers to collect suspended and sinking particles[46]. The latter study reported a significantly lower ratio of TEP to particulate organic carbon (POC) in sinking particles compared to suspended ones. Taken together, these field studies provide environmental corroboration for the biogel-induced particle slowdown proposed here and, together with our proposed mechanism, underscore the pivotal role of biogels in modulating the sinking speed of particles. In turn, by slowing the descent of particles to deeper waters, biogels may extend the duration of microbial remineralization of particulate organic matter in the mesopelagic ocean, enhancing CO_2 recirculation and reducing the amount of carbon that is sequestered in the ocean depths.

In the ocean mixing layer, biofilm aggregates and other biogels serve as a glue that promotes coagulation and aggregation, enhancing the transfer of POC to deeper ocean layers[15,25]. We propose that once particles are below the mixing layer, they intercept and collect suspended biogels and biofilm-producing microorganisms from the surrounding water, thereby changing their own density and hydrodynamic resistance to sinking. Our experiments show that these two effects combined can result in a considerable reduction in sinking speed (Fig. 3C). While direct encounters rather than growth predominantly drove biogel accumulation in our experiments (see details in Supplementary Text, Supplementary Fig. 12, Supplementary Movie 3 and Movie 6), particles in the environment will experience a complex interplay between biogel encounters, biofilm growth on particles, and biogel fragmentation[1,4,5,49,50]. In addition, the dependence of this mechanism on the mechanical properties of biogels implies that particle sinking speed further affects biogel scavenging through the shear forces experienced by biogels. Better insights into and modeling of these processes will yield a more complete understanding of the role of marine biogels on the vertical flux of particles and carbon.

Methods

Endless ocean column

The 'endless-ocean-column' device was designed to continuously image a freely sinking particle over a period of up to 48 h by using a pressure-controlled pump (MFCS -EZ, Fluigent), a video camera, and in-house software to continually adjust the flow rate in a glass column so that the sinking particle remained suspended in front of a vertical microscope (Fig. 1 and Supplementary Fig. 1). A glass tube with square cross-section (VitroCom, S105, 200 × 5 × 5 mm) was used as vertical flow chamber. To suspend the particle, artificial seawater (Instant Ocean with 0.1% MB2216) was supplied at a given flow rate through silicon tubing connected to a 2 L bottle reservoir for input. Note that the flow is through-flow from a reservoir and not a flow round in a circuit. A filter net was attached to the connection between the silicone tubing and the glass tube, and the connection was sealed using Parafilm (PARAFILM® M). A flow-rate platform (Fluigent) equipped with a FLU-L-D flow unit was used to control the flow using an air pressure regulator (MFCS -EZ, Fluigent). The glass tube was illuminated using a circular LED panel (LIU470A, Thorlabs) from the back and was imaged using two USB cameras (Imaging Source DMK23UX250), one frontal, imaging toward the light source, and the other lateral, imaging from the side. The lateral camera (Imaging Source DMK23UX250, equipped with TCL 1616 5MP lens, Imaging source) was stationary and was used to track the position of the particle. The frontal camera provided a magnified image of the suspended particle (18×). This camera was mounted on a 1D-motorized stage (constructed in-house) and was equipped with a zoom lens (0.7–4.5× zoom lens with extension tube; Thorlabs) and 4× objective (CFI Plan Fluor, Nikon). Real-time image analysis and pressure adjustment were performed by an in-house Matlab code. Adjustments to the flow were made in order to maintain the freely sinking particle in a fixed position relative to the camera (see "Sinking experiments" below). To monitor the structure of the particle and the biofilm accumulation around the particle, the frontal camera

acquired a sequence of 40 images every 5 min, where between each of the 40 images, a 25 µm step forward was applied using the 1D-motorized stage, thereby providing a 1 mm *x*-stack of the suspended particle. Each *x*-stack was analyzed using the 'find focused slices' plugin in Fiji (ImageJ). The 1D-motorized stage was controlled by a Raspberry Pi computer.

To test the validity of our endless ocean column system, we calculated the Reynolds number (*Re*) for the column considering a diameter of 5 mm and an average flow velocity of 60 m/day (6.9×10^{-4} m/s), the maximum flow used in the experiments (Fig. 1B, C). Using the kinematic viscosity of seawater at room temperature (9.37×10^{-7} m^2/s at 25 °C, salinity 3.5%), we determined $Re_{max} = 3.7$. Turbulent flow in a tube typically occurs at $Re > 2000$[51], allowing us to conclude that the flow in the column did not become turbulent. The absence of turbulence is further supported by the observed stable orientation of the sinking particles (Supplementary Movie 1 and 6).

To calculate the sinking speed of the particles in the endless ocean column from the average fluid velocity measured by the flow meter, we took three different approaches (Supplementary Fig. 13). (1) Empirical measurements: for 10 particles, we measured the average flow speed in the column required to keep the particle at a fixed height (the approach we have used throughout the study) and compared this value with the actual free-falling speed of the same particle in the same column in the absence of counter-flow. (2) Numerical modeling: we used our numerical model to account for the effects of the no-slip boundary condition on the tube's sidewalls and from it, computed the ratio between the flow velocity at the center of the tube and the average flow velocity. (3) Theoretical prediction: using the analytical solution for flow in a tube with a square cross-section (e.g., Delplace[52]), we again calculated the ratio between the flow velocity at the center of the tube and the average flow velocity. All approaches consistently gave a ratio of approximately 2 (1.88 ± 0.21, 2.13, and 2, respectively) between the local velocity at the column's center and the average flow velocity in the column (Supplementary Fig. 13). We chose to use the empirically measured value of 1.88 ± 0.21 ($n = 10$) to determine the sinking speed of the particle from the measured average velocity of the counter-flow. In addition, we note that the observed stable orientation of all sinking particles indicates that the flow velocity gradients around the particles have no additional discernible effect (Supplementary Movie 1 and 6).

Culture conditions

The diatom *Phaeodactylum tricornutum* strain CCMP 2561 was grown in artificial seawater (Instant ocean, 35 psu) supplemented with f/2 medium (f/2 Media Kit, NCMA Bigelow) under a 12 h: 12 h light:dark cycle at 18 °C. The medium was filtered through a 0.45 µm filter and autoclaved before use. Most experiments in this study were conducted using *Alteromonas macleodii* ATCC27126. Additional bacterial species included *Pseudomonas zhaodongensis* Pz15 and *Vibrio cyclotrophicus* 1F111. The remaining strains, including *Bacillus* sp. F2, were isolated from particles collected from the coast of Massachusetts, USA, and were kindly provided by Otto Cordero's lab (MIT). All bacterial strains in this study were grown at 27 °C in Marine Broth 2216 medium (BD Difco, 279110). Agar plates were made by mixing MB2216 medium with 1% bacteriological agar. Media and plates were autoclaved before use.

Preparation of artificial marine snow particles

Phaeodactylum tricornutum (CCMP 2561) cells were grown in 30 ml f/2 medium in culture flasks for 3 weeks. Cells were then transferred to 20 ml clear glass EPA screw neck vials (ND24, VWR Switzerland, 548-0154) equipped with PP screw caps (ND24 with septum, VWR Switzerland, 548-0872). Vials were placed on a tube roller (Thermo Scientific, 88881004) at 20 rpm for at least 7 days at room temperature to generate phytoplankton aggregates.

Sinking experiments

A single particle was gently picked out of the glass vials using a pipette with 200 µl chopped tip (opening of about 2–3 mm) and placed at the top of the 'endless-ocean-column' millifluidic device. To gain access, the silicon tubing at the top of the 'endless-ocean-column' was detached and replaced after the particle was loaded. The flow was manually adjusted using a syringe pump until the particle migrated to the tracking area in the center of the column, in front of the two cameras. The tracking algorithm was then started, to maintain the freely sinking particle in a stationary position in front of the cameras. This occasionally led to an initial oscillation stage where the particle moved around the center of the image for several minutes. Stable trapping of the particle was usually achieved within 10–60 min. As soon as stable trapping was achieved, the frontal, magnified camera was positioned, and its *x*-position (focus) was optimized. An *x*-stack image was then acquired every 5 min for the duration of the experiment. The particle sinking speed was calculated by multiplying the continuously measured flow rate by an adjustment factor to account for the flow at the center of the tube (see above) and dividing the result by the cross-sectional area of the glass tube (5 × 5 mm).

Experiments were conducted using either low-nutrient sterile artificial seawater (lnASW, ASW supplemented with 0.1% 2216 low-nutrient ASW) or a diluted (1000×) culture of stationary phase *A. macleodii* in lnASW. For experiments with *A. macleodii*, a 2–3 day stationary culture was used as a starter stock (OD = 1.42–1.88), and dilution 1:1000 in lnASW resulted in a final cell count of $(3.1 \pm 1.8) \times 10^9$ CFU per liter. The number of bacteria in the lnASW reservoir after 24 h was found to be $(4.2 \pm 2.2) \times 10^9$ CFU per liter, indicating little to no growth in the reservoir during the course of the experiment. Within this diluted culture, we estimated the concentration of biogel aggregates using microscopy to be about 10-fold lower than that of CFU, since we observed that 90% of colonies that contributed to the CFU count resulted from free-living bacteria rather than biogel aggregates. We note that since *A. macleodii* shows strong biofilm formation during the stationary phase, an optical O.D. measurement fails to provide a reliable and reproducible cell density measurement. Therefore, all cell or biofilm aggregate numbers were inferred from CFU and adjusted based on microscopy as described above.

Visualization of particles in a microfluidic channel

In order to monitor particle colonization underflow in high magnification, a microfluidic chip was used (IBIDI sticky-Slide I, 0.1 mm). An artificial marine snow particle (see above) was placed in the center of the channel and gently covered with a cover slide to trap it. The channel was then slowly filled with ASW using a 1 ml syringe to eliminate all trapped bubbles in the channel. The microfluidic channel was supplied with 1000× diluted *A. macleodii* stationary culture at a rate of 5 µl/min at 25 °C for two days and was visualized using a Nikon Eclipse TI-2 microscope at magnification 150×, capturing phase and fluorescence images at 20 min intervals for 70 h using an Orca flash 4.0 (Hamamatsu) camera. Images were analyzed using NIS-Elements 4.40.00 (Nikon).

Percoll density gradient to determine the density of biofilm and marine particles

A density gradient was prepared by laying Percoll layers (Sigma Aldrich) diluted with artificial seawater on top of each other using a syringe pump. The osmolarity of Percoll was adjusted to that of seawater by adding sea salt (Instant Ocean). The sample was loaded at the top of the Percoll gradient and was centrifuged at 1000 RCF at 22 °C for 10 min. The density of each layer was measured by weighing 1 ml aliquots on scales. All values are the average of three independent measurements.

SEM imaging

For scanning electron microscopy, particles inoculated with *A. macleodii* biofilm were fixed with glutaraldehyde at a final concentration of 2.5% in artificial seawater and attached to a glass support coated with poly-L-lysine. Samples were then washed sequentially for 5 min with 5 ml 2.5% glutaraldehyde, 5 ml ASW, 5 ml 4% osmium tetroxide, and then again with 5 ml ASW. The samples were dehydrated with an ethanol series in deionized water (5 min at each of 30, 50, 70, 90, and 100%), followed by 3 washes with water-free 100% ethanol. The material was critical point dried (Autosamdri-931, Tousimis), and the supports were mounted on aluminum stubs using silver paint. The samples were then sputter-coated with a 4 nm Pt-Pd layer (CCU-010 HV, Safematic) and imaged in a scanning electron microscope (HITACHI SU5000).

Bulk sedimentation measurements

In order to estimate the distributions of sinking speed and size of bacterially treated and untreated particles, a sedimentation tank was constructed (Supplementary Fig. 6). Particles were imaged within a glass column (10 mm × 6 mm × 150 mm, Vitrocom). To quench convective currents, we placed the column within a custom-made acrylic bath (140 mm × 140 mm × 140 mm). An LED panel with a built-in diffuser was placed behind the bath at a distance of 100 mm to provide homogeneous lighting. Imaging was performed at 5 Hz using a CMOS camera (SVS Vistek EXO) with a fixed focal lens (Myutron HF3514V-2), with the camera placed at a distance of 250 mm from the glass chamber. The glass chamber and quenching bath were filled with salt water (3.5% w/v) and left to equilibrate to room temperature for 90 min before each experiment. Once imaging began, 5 µl of the particle-containing solution (see 'preparation of artificial marine snow particles' above) was added to the glass chamber every 5 min for 30 min. The field of view was approximately 25 × 22 mm. Image analysis was performed using an in-house script. After background average subtraction, particle tracking was performed using Trackpy[53]. Tracks were filtered by placing a minimum consecutive image threshold to remove spurious tracks. After preprocessing background-subtracted images using a median filter (size = 3) and binarizing using an Otsu threshold, particle size parameters were obtained from labeled images using the 'skimage' function '*regionprops*'. Tracks from Trackpy and '*regionprops*' size data were matched together to produce a data frame consisting of sinking speed vs particle size.

Determination of biofilm composition using acid fragmentation mass spectrometry analysis

Preparation of biofilm samples. To extract the biofilm, 25 ml of double distilled water (DDW) was added, and the culture was centrifuged at 4500 rcf for 1 min to obtain a biofilm pellet (DDW was added to reduce the density of the culture medium, allowing the suspended biofilm to sink). The supernatant was discarded, and the pellet was washed again with 5 ml DDW and then centrifuged (2 min at 4500 rcf). The DDW wash was performed to promote intra-cellular polysaccharides (IPS) leakage out of the cells, leaving in the pellet primarily the insoluble EPS, however, we cannot rule out the presence of some IPS in our samples, which may thus contain some sugars that originate from IPS rather than EPS. The pellet was then suspended in 8 ml lysis buffer (Tris Buffer 100 mM, pH = 8; EDTA 1 mM pH = 8; NaCl 100 mM in DDW) and vortexed for 10 min until the biofilm dissolved. While solubilization methods may aid in dissolving the EPS within biofilms or extracellular matrices, they can also cause cell lysis, leading to the release of leftover IPS, which differ from EPS in both biological function and chemical composition[54]. Given that IPS does not contribute to biofilm physical properties, its presence could potentially skew EPS monomer profiling. Traditionally, EPS is isolated through filtration or ultracentrifugation to ensure cell-free samples for accurate analysis[55–58]. However, in our case, cell detachment from biofilm was not possible due to the strong adhesion to the EPS. To re-precipitate the biofilm, 42 ml pure ice-cold EtOH was added to the lysis buffer to a final volume of 50 ml, and the solution was vortexed. The biofilm was centrifuged again (2 min, 4500 rcf, 4 °C) to precipitate the polysaccharide fraction. The precipitated biofilm was moved to a 2 ml Eppendorf tube, washed twice with pure EtOH, and centrifuged (2 min, 4500 rcf, 4 °C). To further purify the polysaccharide fraction, the biofilm was then treated with DNAseI for 30 min, then with proteinase K for 30 min, and washed again by EtOH precipitation, keeping the polysaccharide fraction for mass spectrometry analysis. The sample was kept frozen in EtOH until further use.

Acid hydrolysis of purified EPS fractions. Before mass spectrometry, the EtOH was removed, EPS material was suspended in ddH_2O by extensive vortex (10 min, full power) and immediately transferred in triplicates ($n = 3$) of 50 µL of each sample into a PCR plate. The samples were mixed with 50 µL 2 M HCl containing internal standards for LC-MS analysis (2.8 µM fully labeled D-glucose-$13C_6$, D-galactose-$13C_6$, and D-mannose-$13C_6$ with a mass of 186 kDa). Samples were hydrolyzed for 24 h at 100 °C and then adjusted to pH = 7 by the addition of 4 M NaOH.

Derivatization of monosaccharides with 1-phenyl-3-methyl-5-pyrazolone (PMP). Samples containing released monosaccharides after acid hydrolysis (25 µL) were derivatized with 0.1 M PMP in 2:1 methanol:ddH_2O with 0.4 ammonium hydroxide (75 µL) for 100 min at 70 °C following a previously published protocol[59]. For quantification, we derivatized a serial dilution of a standard mix containing galacturonic acid, D-glucuronic acid, xylose, arabinose, D-glucosamine, fucose, glucose, galactose, mannose, N-acetyl-D-glucosamine, ribose, rhamnose, and D-galactosamine.

Quantification of PMP-derivatives with targeted LC-MS. PMP-derivatives were measured on a SCIEX qTRAP5500 and an Agilent 1290 Infinity II LC system equipped with an Agilent Poroshell 120 EC-C18, 2.1 × 50 mm, 1.9 µm reversed-phase column with a guard column. The mobile phase consisted of Buffer A (25 mM NH_4 acetate in ddH_2O, 5% acetonitrile, pH = 5.6 adjusted with formic acid) and Buffer B (5% ddH_2O and 95% acetonitrile). PMP-derivatives were separated in a gradient from 9% to 23% Buffer B in 2 min with a flow of 1 ml/min. The ESI source settings were 625 °C, with curtain gas set to 30 (arbitrary units), collision gas to medium, ion spray voltage 5500 V, temperature to 625 °C, ion source gas 1 to 90, and ion source gas 2 to 90. PMP-derivatives were measured by multiple reaction monitoring (MRM) with previously optimized transitions and collision energies[60]. For example, a glucose derivative has a Q1 mass of 511 and was fragmented with a collision energy of 35 V to yield the quantifier ion of 175 Da and the diagnostic fragment of 217 Da. Different PMP derivatives were identified by their mass and retention compared to known standards, and their peak areas (175 Da fragment) were normalized by the internal standard.

Data availability

All data are available in the main text or the Supplementary Materials. Source data are provided in this paper.

Code availability

The computer codes used during the study are available in Source Data 2.

References

1. Boyd, P. W., Claustre, H., Levy, M., Siegel, D. A. & Weber, T. Multi-faceted particle pumps drive carbon sequestration in the ocean. *Nature* **568**, 327–335 (2019).

2. Iversen, M. H. Carbon export in the Ocean: A biologist's perspective. *Ann. Rev. Mar. Sci.* **15**, 357–381 (2023).
3. Siegel, D. A., DeVries, T., Cetinić, I. & Bisson, K. M. Quantifying the Ocean's biological pump and its carbon cycle impacts on global scales. *Ann. Rev. Mar. Sci.* **15**, 329–356 (2023).
4. Buesseler, K. O. & Boyd, P. W. Shedding light on processes that control particle export and flux attenuation in the twilight zone of the open ocean. *Limnol. Oceanogr.* **54**, 1210–1232 (2009).
5. Briggs, N., Dall'Olmo, G. & Claustre, H. Major role of particle fragmentation in regulating biological sequestration of CO_2 by the oceans. *Science* **367**, 791–793 (2020).
6. Li, F. et al. Planktonic microbial signatures of sinking particle export in the open ocean's interior. *Nat. Commun.* **14**, 7177 (2023).
7. Stephens, B. M. et al. Direct observations of microbial community succession on sinking marine particles. *ISME J* **18**, https://doi.org/10.1093/ismejo/wrad010 (2024).
8. Siegel, D. A. et al. Prediction of the export and fate of global ocean net primary production: The exports science plan. *Front. Mar. Sci.* **3**, 1–10 (2016).
9. Dunne, J. P., Sarmiento, J. L. & Gnanadesikan, A. A synthesis of global particle export from the surface ocean and cycling through the ocean interior and on the seafloor. *Glob. Biogeochem. Cycles* **21**, 1–16 (2007).
10. Martin, J. H., Knauer, G. A., Karl, D. M. & Broenkow, W. W. VERTEX: carbon cycling in the northeast Pacific. *Deep Sea Res. Part A, Oceanogr. Res. Pap.* **34**, 267–285 (1987).
11. Armstrong, R. A., Lee, C., Hedges, J. I., Honjo, S. & Wakeham, S. G. A new, mechanistic model for organic carbon fluxes in the ocean based on the quantitative association of POC with ballast minerals. *Deep Sea Res. Part II: Topical Stud. Oceanogr.* **49**, 219–236 (2001).
12. Alldredge, A. The carbon, nitrogen and mass content of marine snow as a function of aggregate size. *Deep Sea Res. Part I: Oceanogr. Res. Pap.* **45**, 529–541 (1998).
13. Klawonn, I. et al. Fungal parasitism on diatoms alters formation and bio–physical properties of sinking aggregates. *Commun. Biol.* **6**, 206 (2023).
14. Jackson, G. A. A model of the formation of marine algal flocs by physical coagulation processes. *Deep Sea Res. Part A. Oceanogr. Res. Pap.* **37**, 1197–1211 (1990).
15. Burd, A. B. & Jackson, G. A. Particle aggregation. *Ann. Rev. Mar. Sci.* **1**, 65–90 (2009).
16. Nagata, T., Yamada, Y. & Fukuda, H. Transparent exopolymer particles in deep Oceans: Synthesis and future challenges. *Gels* **7**, 75 (2021).
17. Mari, X., Passow, U., Migon, C., Burd, A. B. & Legendre, L. Transparent exopolymer particles: Effects on carbon cycling in the ocean. *Prog. Oceanogr.* **151**, 13–37 (2017).
18. Yamada, Y., Fukuda, H., Inoue, K., Kogure, K. & Nagata, T. Effects of attached bacteria on organic aggregate settling velocity in seawater. *Aquat. Microb. Ecol.* **70**, 261–272 (2013).
19. Yamada, Y. et al. Localized accumulation and a shelf-basin gradient of particles in the Chukchi Sea and Canada Basin, western Arctic. *J. Geophys. Res. Oceans* **120**, 4638–4653 (2015).
20. Verdugo, P. Marine microgels. *Ann. Rev. Mar. Sci.* **4**, 375–400 (2012).
21. Engel, A., Endres, S., Galgani, L. & Schartau, M. Marvelous marine microgels: On the distribution and impact of gel-like particles in the Oceanic water-column. *Front. Mar. Sci.* **7**, https://doi.org/10.3389/fmars.2020.00405 (2020).
22. Bar-Zeev, E., Berman-Frank, I., Girshevitz, O. & Berman, T. Revised paradigm of aquatic biofilm formation facilitated by microgel transparent exopolymer particles. *Proc. Natl Acad. Sci. USA* **109**, 9119–9124 (2012).
23. Kragh, K. N., Tolker-Nielsen, T. & Lichtenberg, M. The non-attached biofilm aggregate. *Commun. Biol.* **6**, 898 (2023).
24. Flemming, H.-C. & Wuertz, S. Bacteria and archaea on Earth and their abundance in biofilms. *Nat. Rev. Microbiol.* **17**, 247–260 (2019).
25. Gärdes, A., Iversen, M. H., Grossart, H. P., Passow, U. & Ullrich, M. S. Diatom-associated bacteria are required for aggregation of *Thalassiosira weissflogii*. *ISME J.* **5**, 436–445 (2011).
26. Simon, M., Grossart, H. H. P., Schweitzer, B. & Ploug, H. Microbial ecology of organic aggregates in aquatic ecosystems. *Aquat. Microb. Ecol.* **28**, 175–211 (2002).
27. Verdugo, P. et al. The oceanic gel phase: A bridge in the DOM-POM continuum. in *Mar. Chem.* **92**, 67–85 (2004).
28. Vernette, C. et al. The Ocean Gene Atlas v2.0: online exploration of the biogeography and phylogeny of plankton genes. *Nucleic Acids Res.* **50**, W516–W526 (2022).
29. Grossart, H. P. et al. Interactions between marine snow and heterotrophic bacteria: Aggregate formation and microbial dynamics. *Aquat. Microb. Ecol.* **42**, 19–26 (2006).
30. Ploug, H. & Jørgensen, B. B. A net-jet flow system for mass transfer and microsensor studies of sinking aggregates. *Mar. Ecol. Prog. Ser.* **176**, 279–290 (1999).
31. Koch, H. et al. Genomic, metabolic and phenotypic variability shapes ecological differentiation and intraspecies interactions of Alteromonas macleodii. *Sci. Rep.* **10**, 809 (2020).
32. Robertson, J. M. et al. Marine bacteria *Alteromonas spp.* require UDP-glucose-4-epimerase for aggregation and production of sticky exopolymer. *mBio* **15**, e00038-24 (2024).
33. Yawata, Y. et al. Competition-dispersal tradeoff ecologically differentiates recently speciated marine bacterioplankton populations. *Proc. Natl. Acad. Sci. USA* **111**, 5622–5627 (2014).
34. Verdugo, P. et al. Marine biopolymer self-assembly: Implications for carbon cycling in the ocean. *Faraday Discuss.* **139**, 393–398 (2008).
35. Mari, X., Beauvais, S., Lemée, R. & Pedrotti, M. L. Non-Redfield C:N ratio of transparent exopolymeric particles in the northwestern Mediterranean Sea. *Limnol. Oceanogr.* **46**, 1831–1836 (2001).
36. Devresse, Q., Becker, K. W. & Engel, A. Distribution of polysaccharidic and proteinaceous gel–like particles in three cyclonic eddies in the Eastern Tropical North Atlantic. *Front. Mar. Sci.* **11**, https://doi.org/10.3389/fmars.2024.1357646 (2024).
37. Gralka, M., Pollak, S. & Cordero, O. X. Genome content predicts the carbon catabolic preferences of heterotrophic bacteria. *Nat. Microbiol.* **8**, 1799–1808 (2023).
38. Stokes, G. G. *On the Effect of the Internal Friction of Fluids on the Motion of Pendulums.* 6 (University Press, Cambridge, 1851).
39. Azetsu-Scott, K. & Passow, U. Ascending marine particles: Significance of transparent exopolymer particles (TEP) in the upper ocean. *Limnol. Oceanogr.* **49**, 741–748 (2004).
40. Friedlander, S. K. Mass and heat transfer to single spheres and cylinders at low Reynolds numbers. *AIChE J.* **3**, 43–48 (1957).
41. Mari, X. & Burd, A. Seasonal size spectra of transparent exopolymeric particles (TEP) in a coastal sea and comparison with those predicted using coagulation theory. *Mar. Ecol. Prog. Ser.* **163**, 63–76 (1998).
42. Myklestad, S. M. Release of extracellular products by phytoplankton with special emphasis on polysaccharides. *Sci. Total Environ.* **165**, 155–164 (1995).
43. Seebah, S., Fairfield, C., Ullrich, M. S. & Passow, U. Aggregation and sedimentation of *Thalassiosira weissflogii* (diatom) in a warmer and more acidified future Ocean. *PLoS ONE* **9**, e112379 (2014).
44. Tréguer, P. et al. Influence of diatom diversity on the ocean biological carbon pump. *Nat. Geosci.* **11**, 27–37 (2018).
45. Romanelli, E., Sweet, J., Giering, S. L. C., Siegel, D. A. & Passow, U. The importance of transparent exopolymer particles over ballast in determining both sinking and suspension of small particles during late summer in the Northeast Pacific Ocean. *Elem. Sci. Anth.* **11**, https://doi.org/10.1525/elementa.2022.00122 (2023).

46. Yamada, Y. et al. Functions of extracellular polymeric substances in partitioning suspended and sinking particles in the upper oceans of two open ocean systems. *Limnol. Oceanogr.* https://doi.org/10.1002/lno.12554 (2024).
47. Chajwa, R., Flaum, E., Bidle, K. D., Van Mooy, B. & Prakash, M. Hidden comet tails of marine snow impede ocean-based carbon sequestration. *Science* **386**, eadl5767 (2024).
48. Krishnamurthy, D. et al. Scale-free vertical tracking microscopy. *Nat. Methods* **17**, 1040–1051 (2020).
49. Nguyen, T. T. H. et al. Microbes contribute to setting the ocean carbon flux by altering the fate of sinking particulates. *Nat. Commun.* **13**, 1657 (2022).
50. Alcolombri, U. et al. Sinking enhances the degradation of organic particles by marine bacteria. *Nat. Geosci.* **14**, 775–780 (2021).
51. Avila, K. et al. The onset of turbulence in pipe flow. *Science* **333**, 192–196 (2011).
52. Delplace, F. Laminar flow of Newtonian liquids in ducts of rectangular cross-section a model for both physics and mathematics. *Open Access J. Math. Theor. Phys.* **1**, 198–201 (2018).
53. Allan, D. B., Caswell, T., Keim, N. C., van der Wel, C. M. & Verweij, R. W. soft-matter/trackpy: Trackpy v0.5.0 https://doi.org/10.5281/ZENODO.4682814 (2021).
54. Liu, Y. et al. Preparation and characterization of intracellular and exopolysaccharides during cycle cultivation of *Spirulina platensis*. *Foods* **12**, 1067 (2023).
55. Aslam, S. N., Cresswell-Maynard, T., Thomas, D. N. & Underwood, G. J. C. Production and characterization of the intra- and extracellular carbohydrates and polymeric substances (EPS) of three sea-ice diatom species, and evidence for a cryoprotective role for EPS. *J. Phycol.* **48**, 1494–1509 (2012).
56. Kumar, M. A., Anandapandian, K. T. K. & Parthiban, K. Production and characterization of exopolysaccharides (EPS) from biofilm forming marine bacterium. *Braz. Arch. Biol. Technol.* **54**, 259–265 (2011).
57. Rizzo, C. et al. Characterization of the exopolymer-producing *Pseudoalteromonas* sp. S8-8 from Antarctic sediment. *Appl. Microbiol. Biotechnol.* **106**, 7173–7185 (2022).
58. Srivastava, N., Kumari, S., Kurmi, S., Pinnaka, A. K. & Choudhury, A. R. Isolation, purification, and characterization of a novel exopolysaccharide isolated from marine bacteria *Brevibacillus borstelensis* M42. *Arch. Microbiol* **204**, 399 (2022).
59. Rühmann, B., Schmid, J. & Sieber, V. Fast carbohydrate analysis via liquid chromatography coupled with ultra violet and electrospray ionization ion trap detection in 96-well format. *J. Chromatogr. A* **1350**, 44–50 (2014).
60. Xu, G., Amicucci, M. J., Cheng, Z., Galermo, A. G. & Lebrilla, C. B. Revisiting monosaccharide analysis – quantitation of a comprehensive set of monosaccharides using dynamic multiple reaction monitoring. *Analyst* **143**, 200–207 (2018).

Acknowledgements

We thank Dr. Russell Naisbit for his help with editing the manuscript and members of the Simons Foundation PriME collaboration for fruitful discussions. We gratefully acknowledge funding from the European Molecular Biology Organization (EMBO; ALTF 1109-2016), from the Human Frontier Science Program (HFSP; LT001209/2017) and Alon scholarship (Council for Higher Education, Israel) to U.A.; from an ETH Postdoc Fellowship to A.N.; from the European Union's Horizon 2020 research and innovation program under a Marie Skłodowska-Curie grant agreement (No. 798411) to F.J.P.; from a Swiss National Science Foundation Ambizione Grant (PZ00P2_202188) to J.S.; from a Swiss National Science Foundation PRIMA Grant (No. 179834) to E.S.; from the Luxembourg National Research Fund's ATTRACT Investigator Grant (Grant no. A17/MS/11572821/MBRACE) and CORE Grant (C19/MS/13719464/TOPOFLUME/Sengupta) to A.S.; and from a Gordon and Betty Moore Foundation Symbiosis in Aquatic Systems Initiative Investigator Award (GBMF9197), and from the Simons Foundation through the Principles of Microbial Ecosystems (PriME) collaboration (grant 542395FY22) to R.S.

Author contributions

U.A. and R.S. designed research; U.A., D.A.B., A.Se., and K.S.L. designed and fabricated the experimental setups; U.A., S.C., I.S., A.S., A.Se., and E.S. conducted experiments; U.A. analyzed data; U.A., A.N., J.S., F.J.P, A.S., U.S., A.Se., and R.S. interpreted results. U.A., A.N., J.S., F.J.P., and R.S. designed and developed mathematical models; A.N. performed numerical simulations; U.A., A.N., J.S., and R.S. wrote and revised the paper, with input from all authors.

Competing interests

The authors declare no competing interests.

Additional information

Supplementary information The online version contains supplementary material available at https://doi.org/10.1038/s41467-025-57982-5.

Correspondence and requests for materials should be addressed to Uria Alcolombri or Roman Stocker.

Peer review information *Nature Communications* thanks Matthew J. Rau, who co-reviewed with David Fierli and the other anonymous reviewer(s) for their contribution to the peer review of this work. A peer review file is available.